

Palladium nanoparticles passivated by metal–carbon covalent linkages†

Debraj Ghosh and Shaowei Chen*

Received 8th October 2007, Accepted 28th November 2007

First published as an Advance Article on the web 10th January 2008

DOI: 10.1039/b715397j

Stable palladium nanoparticles were prepared by the passivation of palladium–carbon covalent linkages by the reduction of diazonium derivatives. The resulting particles were characterized by TEM, UV-vis, FTIR, and NMR measurements. Interestingly, in electrochemical studies of the electronic conductivity of the particle solid ensembles, Pd–biphenyl particles exhibited metallic temperature dependence within the temperature range of 80 to 320 K; whereas the conductivity of Pd–decylphenyl particles showed a transition from semiconductor to metal at 180 K, manifested by their distinctly different temperature dependence. Control experiments with alkanethiolate-protected palladium nanoparticles in the same temperature range exhibited only semiconductor-like conductivity which increased with increasing temperature. The discrepancy was interpreted using Mott's model for metal–insulator transition and ascribed to the strong Pd–C interactions and low contact resistance, which facilitated the interparticle charge transfer.

Introduction

The research interest in nanosized metal particles has been primarily motivated by the unique material properties that may be exploited for diverse applications, such as nano-electronics, (electro)catalysis, chemical/biological sensing, *etc.*^{1–4} Of these, monolayer-protected nanoclusters (MPCs) represent an intriguing class of nanomaterials whose properties can be manipulated readily and independently by the structure of the metal cores as well as the organic capping shells.^{1,2,5,6} In the chemical synthesis of MPCs, the growth dynamics of the particles has been found to be controlled by at least two competing processes,⁷ nucleation of zero-valence metal atoms to form the cores, and passivation of surfactant ligands to limit the growth of the cores. Thus, the choice of the organic capping ligands plays a critical role in the regulation of the nanoparticle structures and hence their chemical/physical properties and functional applications. In these studies, alkanethiols and other thiol derivatives have been used extensively as the ligands of choice to stabilize metal nanoparticles by taking advantage of the strong affinity of the thiol groups for transition metal surfaces.^{8–12}

Recently, transition-metal nanoparticles protected by other capping groups have also been reported. For instance, stable ruthenium nanoparticles have been prepared by the passivation of Ru=C double bonds by virtue of the carbene fragments formed by the reduction of diazo derivatives.¹³ Metal–carbon single-bond linkages have also been exploited to stabilize gold and platinum nanoparticles by using diazonium derivatives as the precursors.¹⁴ Yet, to the best of our knowledge, such unique chemistry has not been extended to other transition metal nanoparticles.

For instance, various synthetic protocols have been developed for the preparation of palladium nanoparticles, *e.g.*, vapor condensation,¹⁵ sonochemical reduction,^{16,17} chemical liquid deposition,¹⁸ reflux alcohol reduction,^{19–22} decomposition of organometallic precursors,²³ hydrogen reduction,²⁴ electrochemical deposition,^{25–27} and the biphasic Brust protocol^{18,28,29} (a more extensive survey of particle synthetic protocols can be found in a recent review³⁰). Yet, in these earlier studies, the particles are mostly stabilized by polymers through noncovalent interactions or thiol derivatives by virtue of the Pd–S linkage. Little attention has been paid to palladium nanoparticles that are passivated by palladium–carbon covalent bonds. As palladium has been used extensively as the contact metal of choice in the fabrication of carbon nanotube-based nanoelectronic devices/circuitries because of the low contact resistance,^{31–33} one would anticipate that palladium–carbon covalent linkages will be strong enough to stabilize the nanosized particles. In fact, the bonding energy for a Pd–C single bond is 436 kJ mol⁻¹, even larger than that of the Pd–S linkage (380 kJ mol⁻¹).³⁴ Thus, fundamentally, it will be of great interest to examine the effect of the metal–ligand bonding interactions on the particle charge transfer properties, because of the metal–organic composite nature of the nanoparticle materials, and because nanoparticles are playing an increasingly important role in nanoelectronics. This is the primary motivation of this work.

In this study, we first report the synthesis and characterization of a series of palladium nanoparticles that are protected by Pd–C single bonds (hence referred to as Pd–C particles), and examine the solid-state electronic conductivity of the particle dropcast films. In contrast to the semiconductor characters that are generally manifested by alkanethiolate-protected palladium (Pd–SR) nanoparticles, the conductivity properties of the Pd–C particles are markedly different. For instance, for biphenyl-stabilized Pd particles, the temperature dependence of the ensemble conductivity is consistent with metallic materials; whereas for decylphenyl-protected particles, the ensemble conductivity exhibits a transition from semiconductor to metal with increasing

Department of Chemistry and Biochemistry, University of California, 1156 High Street, Santa Cruz, California 95064, USA. E-mail: schen@chemistry.ucsc.edu

† Electronic supplementary information (ESI) available: TEM micrographs of thiolate-protected palladium nanoparticles and their corresponding *I–V* profiles. See DOI: 10.1039/b715397j

temperature. This indicates the importance of metal-carbon linkages in the regulation of interparticle charge transfer, in addition to the specific chemical structure of the linkers.

Experimental

Chemicals

Palladium chloride (PdCl_2 , 96%, ACROS), tetra-*n*-octylammonium bromide (TOABr, 98%, Aldrich), hydrochloric acid (HCl, Fisher), superhydride ($\text{Li}(\text{C}_2\text{H}_5)_3\text{H}$, 1 M in THF, ACROS), fluoroboric acid (HBF_4 , 50 wt% in water, ACROS), 4-ethylaniline (99+%, ACROS), 4-decylaniline (ACROS), 4-aminobiphenyl (Aldrich), sodium nitrite (NaNO_2 , p.a., ACROS), *n*-hexanethiols (C6SH, 96%, Aldrich), *n*-decanethiol (C10SH, 96%, Aldrich), *n*-dodecanethiol (C12SH, 98.5%, Aldrich), and all solvents (from ACROS) were used as received. Water was supplied with a Barnstead Nanopure water system (18.3 M Ω cm).

Synthesis of Pd nanoparticles

Diazonium ligands were synthesized by following a literature synthetic protocol.³⁵ Briefly, a calculated amount of an amine precursor was dissolved in ice-cold 50 wt% fluoroboric acid, to which a 1 : 1 stoichiometric amount of sodium nitrite was added. The solution was allowed to mix for several minutes. The products were then washed thoroughly with cold fluoroboric acid, ethanol, and ether to remove any impurities, affording the corresponding compounds of diazonium tetrafluoroborate. Three batches of diazonium ligands were prepared in this study using 4-ethylaniline, 4-decylaniline, and 4-aminobiphenyl as the precursors, which were then used to prepare stable palladium nanoparticles as detailed below.

The procedure for the synthesis of the Pd nanoparticles varied slightly with the diazonium ligands used. To prepare decylphenyl- and biphenyl-stabilized palladium nanoparticles (denoted as Pd-DP and Pd-BP, respectively), we adopted the synthetic procedure that was used previously for the synthesis of gold and platinum nanoparticles.¹⁴ Briefly, palladium chloride (0.25 mmol) was dissolved in 50 mL of nanopure water; and a calculated amount of the diazonium salt was dissolved in 50 mL of toluene. These two solutions were then mixed under rigorous magnetic stirring for about 30 min. The aqueous phase was found to become colorless whereas the organic phase turned orange-brown, signifying that the Pd(II) ions were transferred into the organic phase by complexation with the diazonium ions. The aqueous phase was separated and discarded. Superhydride ($\text{Li}(\text{C}_2\text{H}_5)_3\text{BH}_4$, 5 mL) was then added dropwise to the organic phase. The solution color changed rapidly from orange to dark green-black signifying the formation of palladium nanoparticles. The solution was allowed to stir for another 30 min, and then washed twice with 0.5 M sulfuric acid and twice with 0.5 M sodium bicarbonate to remove any unreacted metal complexes. Subsequently, solvents were removed under reduced pressure with a rotary evaporator. The resulting sample was washed several times with ethanol to remove any excess of ligands and other impurities. In this study, the Pd-DP particles were prepared at a Pd : diazonium molar feed ratio of 1 : 2, and for Pd-BP 1 : 4; thus the resulting particles are referred to as Pd-DP (2 \times) and Pd-BP (4 \times) respectively.

To prepare palladium nanoparticles stabilized by ethylphenyl ligands (denoted as Pd-EP), the synthetic procedure was slightly different. Here, palladium chloride (0.25 mmol) was first dissolved in 0.5 M HCl. To this solution was then added 1.1 g of tetraoctylammonium bromide in 80 mL of dichloromethane to transfer Pd(II) to the organic phase. The aqueous phase was then removed and the organic phase was washed three times with nanopure water. The organic solution was bright orange in color. A calculated amount of the ethylphenyldiazonium ligands was then added to the organic solution. The formation of the palladium nanoparticles occurred upon the dropwise addition of 5 mL superhydride ($\text{Li}(\text{C}_2\text{H}_5)_3\text{BH}_4$) where the solution color changed from bright orange to dark green-black. Then the washing protocol used above for the Pd-BP and Pd-DP particles was employed for the purification of the Pd-EP particles. Two sets of Pd-EP nanoparticles were prepared, one with a palladium : diazonium (molar) feed ratio of 1 : 2 (2 \times), and the other 1 : 4 (4 \times).

The particles synthesized above all exhibited good solubility in apolar solvents (*e.g.*, CH_2Cl_2 , CHCl_3 , THF, and toluene) but were insoluble in polar solvents such as alcohols and acetone. Yet it was found that the two batches of Pd-EP particles gradually lost their solubility in apolar solvents when exposed to air for an extended period of time whereas the Pd-DP and Pd-BP particles were quite stable. Thus the characterizations of the Pd-EP particles were limited to TEM, UV-vis and FTIR measurements of their fresh samples.

For comparison, palladium nanoparticles have also been prepared by using alkanethiolates as the protecting ligands (all at a Pd : thiol feed ratio of 1 : 2). Specifically, hexanethiolate-, decanethiolate-, and dodecanethiolate-protected palladium nanoparticles (denoted as Pd-SC6, Pd-SC10 and Pd-SC12 respectively) were synthesized by using the procedure that was described previously.²⁸

Spectroscopies

Transmission electron microscopic (TEM) measurements were carried out with a JEOL 1200 EX transmission electron microscope operated at 80 keV. The samples were prepared by casting a drop of the particle solutions in toluene onto a 200-mesh carbon-coated copper grid; and at least five images were acquired for each sample. High-resolution TEM micrographs were acquired at the National Center for Electron Microscopy at the Lawrence Berkeley National Laboratory. The nanoparticle core sizes were estimated by digitizing the TEM micrographs with ImageJ[®] software.

The purity of the nanoparticles was confirmed by proton NMR measurements (Varian Unity 500 MHz) which were carried out with concentrated solutions of the nanoparticles dissolved in CDCl_3 . The absence of any sharp features indicated that the particles were free of excessive free ligands. UV-visible spectroscopic measurements were carried out with a UNICAM ATI UV4 spectrometer. The particles were typically dissolved in CH_2Cl_2 at a concentration of 0.1 mg mL⁻¹. The FTIR measurements were carried out with a Perkin-Elmer FTIR spectrometer (Spectrum One) where the samples were prepared by casting the particle solutions onto a NaCl disk. The spectral resolution was 4 cm⁻¹.

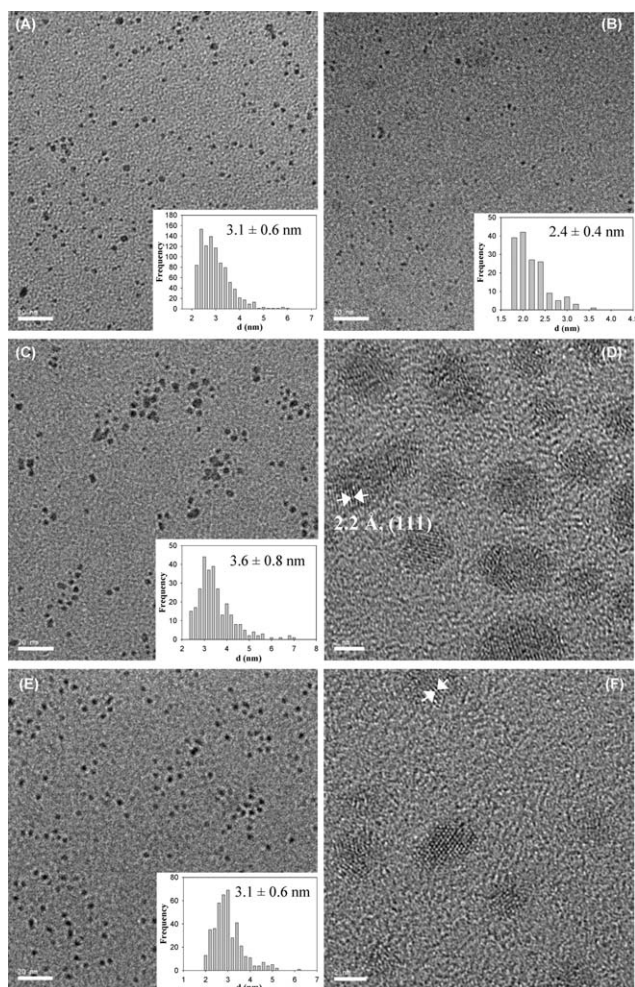


Fig. 1 TEM micrographs of (A) Pd-EP (2 \times), (B) Pd-EP (4 \times), (C) and (D) Pd-DP (2 \times), and (E) and (F) Pd-BP (4 \times) particles. Scale bars in (A), (B), (C) and (E) are 20 nm; and in (D) and (F), 2 nm. Insets show the respective histograms of the nanoparticle size distribution. Arrows denote the lattice fringes obtained in high-resolution TEM measurements (D and F).

Electrochemistry

The solid-state conductivity of the nanoparticles was measured by electrochemical studies of their “dropcast” films. Here a concentrated solution (typically 50 mg mL⁻¹ in toluene) of the palladium nanoparticles was deposited onto the fingers of a gold interdigitated arrays (IDA) electrode (25 pairs of gold fingers of 3 mm \times 5 μ m \times 5 μ m, from ABTECH) by using a Hamilton microliter syringe. The electrode was then placed inside a cryostat vacuum chamber (from Janus Research Company) and the current–potential profiles were collected by using a CHI 440

potentiostat with the temperature varied from 80 to 320 K (Lakeshore Temperature Controller Model 331). The ensemble conductivity (σ) was evaluated by using the equation

$$\sigma = \left(\frac{1}{49R} \right) \left(\frac{S}{L} \right)$$

where R is the ensemble resistance calculated from the slope of the I – V curves, L is the IDA electrode interfinger gap (5 μ m); and S is the film cross-section area approximated by (finger height, 5 μ m) \times (finger length, 3 mm). The constant (49) reflects that there are totally 49 junctions which are in parallel within the IDA chip.

Results and discussion

TEM measurements

Transmission electron microscopy (TEM) has been used extensively to examine the nanoparticle core dimensions and structures.^{36,37} Fig. 1 shows a representative TEM micrograph for each of the Pd nanoparticles stabilized by Pd–C linkages. First, it can be seen that the particles were dispersed thoroughly over the entire grid without any apparent aggregation, suggesting sufficient passivation of the Pd nanoparticle cores by the aliphatic ligands through the Pd–C bonds, akin to the Pt–C and Au–C particles reported earlier.¹⁴ Second, high-resolution TEM images (panels D and F) clearly depict a lattice fringe of 2.2 Å which is consistent with the spacing of the Pd(111) single crystal lattice. Third, from the core size histograms (insets), the majority of the particles can be found within the size range of 2 to 4 nm; and the series of nanoparticles all exhibit a rather narrow dispersity (\sim 20%) of the core diameter, as summarized in Table 1. Overall, the core size (and dispersity) is rather comparable to that of the platinum nanoparticles (dia. \sim 3 nm) synthesized under similar conditions, but substantially smaller than that of the gold counterparts (*ca.* 8 nm).¹⁴ This can be ascribed to the weak Au–C bond (<200 kJ mol⁻¹)³⁸ as compared to the Pt–C (598 kJ mol⁻¹) and Pd–C (436 kJ mol⁻¹) counterparts,³⁴ as the metal–ligand bond strength largely dictates the passivation of the core during particle growth.⁷

In addition, in the Pd–EP particles (Fig. 1, panels A and B), it can be seen that by increasing the initial feed ratio of diazonium to palladium, the average diameter of the resulting particles decreases somewhat, from 3.1 \pm 0.6 nm (2 \times) to 2.4 \pm 0.4 nm (4 \times). This is in good agreement with previous results³⁹ where a larger excess of protecting ligands results in a smaller diameter of the particle core, as a consequence of the competing mechanism in nanoparticle growth.⁷ Yet, it should be noted that a large excess of alkanethiols will corrode the Pd cores, leading to the formation of ionic complexes,^{28,29} whereas the Pd–C particles obtained above remain stable in the presence of excessive

Table 1 Summary of the core diameter (d) of Pd nanoparticles stabilized by different surface monolayers

| | Particles | | | | | | |
|-------------------|---------------|---------------|---------------|---------------|---------------|---------------|---------------|
| | Pd-EP | | Pd-DP | Pd-BP | Pd-SC6 | Pd-SC10 | Pd-SC12 |
| Pd : ligand ratio | (2 \times) | (4 \times) | (2 \times) | (4 \times) | (2 \times) | (2 \times) | (2 \times) |
| d /nm | 3.1 \pm 0.6 | 2.4 \pm 0.4 | 3.6 \pm 0.8 | 3.1 \pm 0.6 | 3.5 \pm 0.6 | 3.9 \pm 0.9 | 5.0 \pm 1.4 |

diazonium, again suggesting a rather dense packing of the aliphatic ligands on the particle surface.

The TEM micrographs and core size histograms for the three alkanethiolate-protected palladium (Pd-SR) particles are included in the Electronic Supplementary Information (ESI† Fig. S1). The average core diameters are found to be between 3 and 5 nm (Table 1), slightly larger than the Pd-C particles (Table 1). Again, this may be ascribed to the stronger Pd-C linkage and hence more effective passivation of the particle surface during nanoparticle growth.⁷

Spectroscopy

Nanometer-sized transition-metal particles exhibit unique optical properties.⁴⁰ For example, Au, Ag, and Cu nanoparticles exhibit intense surface plasmon resonances in the visible range which are superimposed onto the exponential-decay Mie-scattering spectra. In the case of nanoscale palladium particles, however, the absorption profile does not exhibit a surface-plasmon resonance band. Indeed, the UV-vis absorption spectra of the Pd-C nanoparticles synthesized above (not shown) are all featureless with only an exponential decay profile, very similar to those of the Pd-SR nanoparticles,²⁸ as interpreted by the Mie theory.⁴⁰

Fig. 2 depicts the FTIR spectra of the three Pd-C nanoparticles, along with those of their respective diazonium compounds. It can be seen that the majority of the vibrational features remain almost the same for both the Pd-C particles and the corresponding diazonium ligands. These include, for instance, the C=C stretches in the aromatic rings at 686, 729, 1500, and 1608 cm^{-1} , and methylene C-H stretches at 2880 and 2939 cm^{-1} .⁴¹ Yet, the most striking difference is the disappearance of the diazonium (N≡N) vibrational stretch at 2250 cm^{-1} in the particle samples as compared to the results of the free ligands. Similar behavior has also been observed previously in the synthesis of Au-C and Pt-C nanoparticles.¹⁴ Upon the addition of the reducing agent, nitrogen was released as a consequence of the reduction (and cleavage) of the diazonium moieties; and the resulting aliphatic radicals bound to the Pd surface forming Pd-C bonds. Thus, from the FTIR results (Fig. 2) one can also see that the particle samples are free of excessive diazonium ligands.

The purity of the Pd-C nanoparticles was further examined by ¹H NMR measurements. Fig. 3 shows the spectra of both the Pd-DP and Pd-BP particles along with their respective diazonium ligands in CDCl₃. First, it can be seen that in decylphenyldiazonium (panel D), the four phenyl protons can be clearly identified at 7.6 (2H) and 8.6 (2H) ppm; additional characteristic peaks can be observed at 0.9 ppm and 1.2 ppm for the methyl and methylene protons, respectively. For biphenyldiazonium (panel B), the nine phenyl protons can be found at the three peaks between 7.4 and 7.7 ppm. Yet, when the ligands are bound onto the Pd particle surface, the responses become drastically different. For the Pd-DP particles (panel C), only the peaks for the methyl and methylene protons can now be seen and they are substantially broadened, as compared to their counterparts in the free ligands (panel D); whereas the peaks for the phenyl protons vanish completely. The phenyl protons cannot be seen in the Pd-BP nanoparticles either (panel A). This is because the peaks simply become broadened into the baseline. This broadening phenomenon has been observed previously with other nanoparticles and

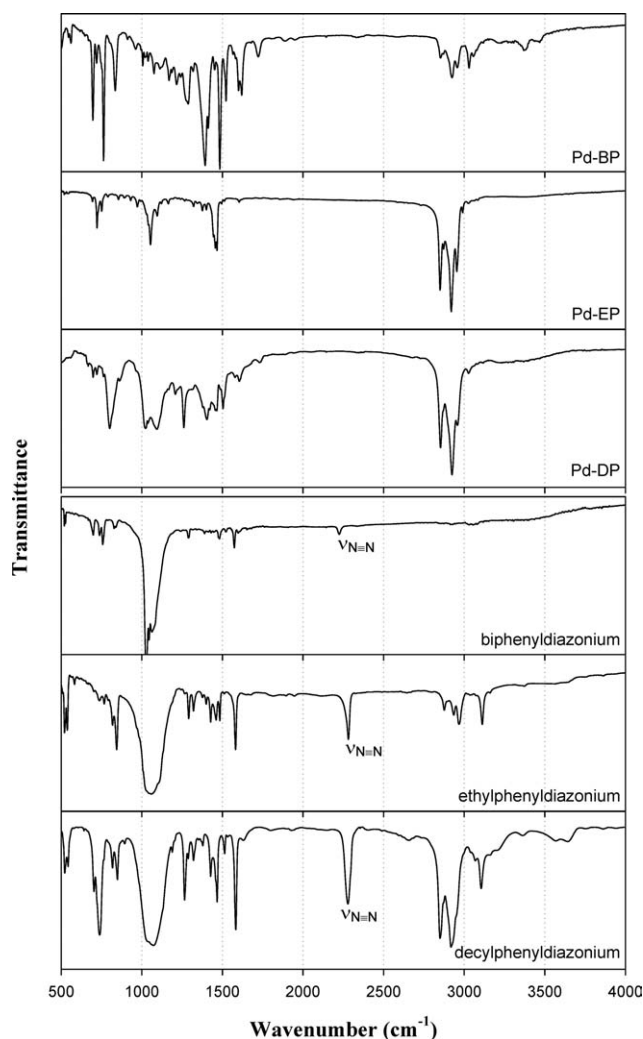


Fig. 2 FTIR spectra of the three diazonium ligands and the corresponding palladium nanoparticles. Samples were prepared by dropcasting their respective concentrated solutions in dichloromethane onto a NaCl disk.

accounted for by the combined effects of several factors, including the slow tumbling rate of the nanoparticles, and heterogeneous packing density and conformations of the ligands on the particle surface.^{42,43} In reality, the broadening becomes more pronounced as the functional group lies closer to the particle core; and hence the disappearance of the phenyl protons in the aforementioned Pd-C particles. The broadened features can also be used as a signature to distinguish particle-bound ligands from the free ones. Thus, the absence of any sharp feature in the high field region (>7 ppm) in the particle NMR spectra strongly suggests that the obtained particles are free of any free diazonium ligands or their reduced products (note that the sharp peaks at *ca.* 7.2 ppm and 1.5 ppm are from the CDCl₃ solvent; and peaks at lower fields most likely arise from traces of solvents from the particle purification process, such as CH₂Cl₂ at 5.3 ppm, and ethanol and acetone at 2–3 ppm).

Conductivity studies

The solid-state conductivity of the Pd-C nanoparticles obtained above was then examined by electrochemical measurements with

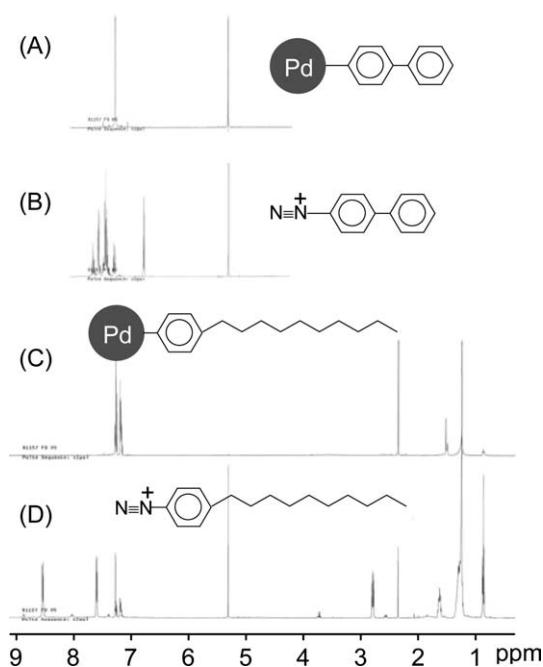


Fig. 3 ^1H NMR spectra of Pd–C nanoparticles (A, Pd–BP; C, Pd–DP) and diazonium ligands (B, biphenyldiazonium; D, decylphenyldiazonium). The samples were all prepared in CDCl_3 .

a dropcast thick film of the particles on an IDA electrode. Fig. 4A shows the current–potential (I – V) profiles of the Pd–BP nanoparticles within the temperature range of 80 to 290 K. It can be seen that the I – V responses exhibit a linear (ohmic) character within the entire temperature range under study, suggesting very efficient interparticle charge transfer. This is not surprising, considering the short and aromatic capping layer. As compared to the control measurements with the same blank electrode (current of the order of pA; red dotted line), the currents of the particle solid films are significantly greater, of the order of mA even at a potential bias of only ± 0.4 V. More importantly, the currents are found to decrease with increasing temperature (80 K to 320 K), behavior actually anticipated for metallic materials.³⁴ From the slope of the I – V curves, one can calculate the conductivity of the particle solid films which is

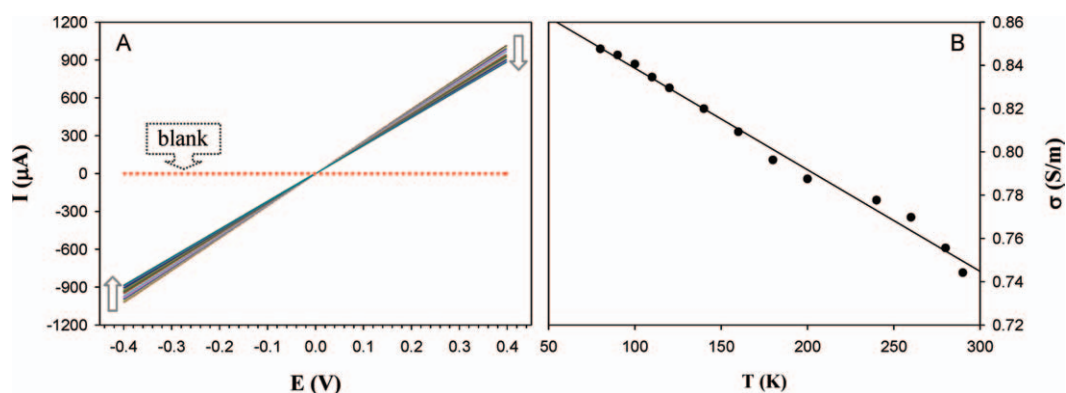


Fig. 4 (A) Current–potential profiles of a Pd–BP nanoparticle dropcast thick film at varied temperature. Potential scan rate 20 mV s^{-1} . (B) Variation of the ensemble conductivity with temperature.

only slightly less than 1 S m^{-1} (Fig. 4B). This is about seven orders of magnitude smaller than that of bulk palladium (*ca.* $0.93 \times 10^7 \text{ S m}^{-1}$ at room temperature³⁴), which can be ascribed to the metal–organic nanocomposite nature of the particles. Additionally, the particle conductivity decreases (almost linearly) with temperature in the range of 80 to 290 K (Fig. 4B). While the decrease is less dramatic than that of the bulk metal, the observation deviates significantly from previous studies^{44–48} of metal nanoparticles protected with thiol derivatives where the conductivity is generally found to increase with increasing temperature, namely, the particle ensembles behave as semiconductor materials and the interparticle charge transfer (hopping) is interpreted on the basis of a thermal activation mechanism (ESI†).

As the average core diameter of the Pd–BP nanoparticles is $\sim 3 \text{ nm}$ (Table 1 and Fig. 1), the particle cores will behave similarly to bulk palladium. Thus, the ensemble conductivity is anticipated to be mainly determined by the Pd–ligand contact and the ligand matrix itself. Yet, as mentioned earlier, palladium has been used extensively as the metal of choice to create contacts with carbon nanotubes because of the strong Pd–C bonding interactions and low contact resistance.^{31–33} Furthermore, the π – π stacking as a result of ligand intercalations between adjacent particles in the solid films may serve as an effective pathway for interparticle charge transfer.⁴⁹ Thus, it is most probable that the combination of all these factors gives rise to the metal-like conductivity properties of the Pd–BP particle solids.

By introducing a saturated spacer into the capping ligands, the resulting particles exhibit drastic differences in the I – V measurements. Fig. 5 (panels A and B) depicts the I – V data of the Pd–DP particles. First, linear I – V profiles can also be seen within the entire temperature range of 80 to 320 K (Fig. 5), but the magnitude of the currents (of the order of tens of nA) is substantially smaller than that observed above with the Pd–BP particles (Fig. 4), although they are still significantly larger than the background currents (red dotted line in panel A). This can be ascribed to the long decyl spacer that impedes interparticle charge transfer.

Second, in contrast to the Pd–BP particles which exhibit a monotonic decrease of the ensemble conductivity with increasing temperature (Fig. 4), the Pd–DP particles behaves somewhat more complicated. From Fig. 5A, one can see that the current first increases with increasing temperature from 80 to 180 K, exhibiting semiconductor character; yet, with further increase

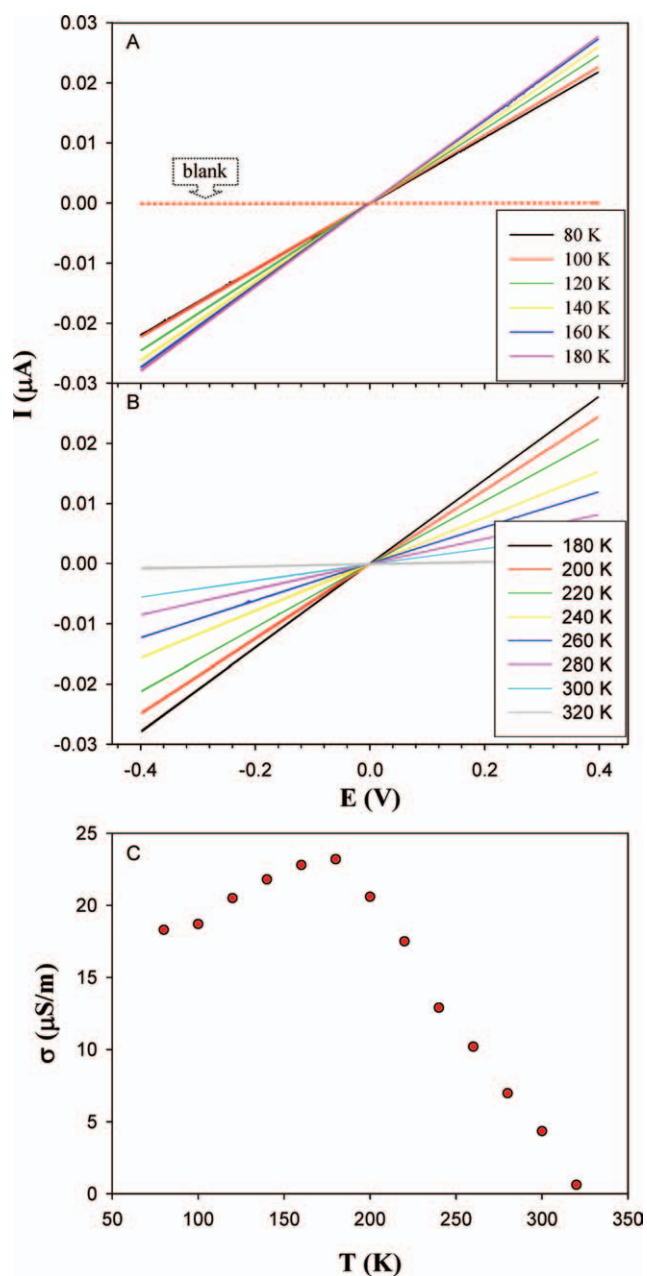


Fig. 5 (A and B) Current–potential profiles of a Pd–DP nanoparticle dropcast thick film at varied temperature. Potential scan rate 20 mV s^{-1} . (C) Variation of the ensemble conductivity with temperature.

of the temperature (from 180 to 320 K), the current actually starts to decrease (panel B), akin to that observed in Fig. 4 where the particle films behaves like metallic materials instead. Fig. 5C summarizes the ensemble conductivity with temperature, and it clearly depicts a transition temperature around 180 K where the interparticle charge transfer evolves from semiconductor to metallic behavior.

It has to be noted that in the above studies, the particles could be recovered completely from the IDA electrode surface by dissolving them in CH_2Cl_2 at the end of the measurements, and the I – V responses of the IDA electrode remained virtually invariant to that prior to the deposition of the particle films.

This suggests little ripening of the particles after repetitive potential cycling. Thus, it is highly unlikely that the metallic character observed above arose from ligand desorption and consequently direct contact of the particle cores and shortening of the IDA fingers.

Similar transitions have also been reported in resistivity measurements of monolayers of much larger Ag nanoparticles (dia. 7.8 nm) passivated by octanethiolates or decanethiolates⁵⁰ where at temperatures above 200 K the films exhibit a metal-like resistance, whereas at lower temperatures (60 to 200 K) the conductance is mainly driven by thermal activation and the films behave as semiconductors. Heath and co-workers explained this behavior by using the Mott–Hubbard band model. At low temperatures, the particle superlattice is a Mott insulator with a Coulomb gap that originates from the single particle charging energy (*i.e.*, the Hubbard energy); whereas at higher temperatures, metallic behavior starts to emerge where the interparticle charge transfer is facilitated as a result of the temperature-induced band widening. Using a scattering formalism, Remacle and Levine⁵¹ carried out a computational study to examine the current–potential–temperature characteristics of these nanoparticle ensembles; and the temperature-dependent conductivity was attributed to the increase of the number of energy states that contributed to the interparticle charge transfer.

In another study, Snow and Wohltjen⁴⁷ measured the conductance of solid films of dodecanethiolate-stabilized gold nanoparticles of varied sizes. For particles with core diameter $<5.0 \text{ nm}$, only semiconductor-like temperature dependence was observed of the ensemble conductivity within the temperature range of 190 to 300 K; whereas for larger particles (core dia. *ca.* 6.0 nm and 7.2 nm) the ensemble conductivity was found to evolve from semiconductor to metallic behavior with increasing temperature, and the transition temperature decreased with increasing particle core size, from 260 K (6.0 nm) to 240 K (7.2 nm). Two mechanisms were employed to account for such a transition. One is related to the shrinking of the particle core to the domain of the de Broglie wavelength; and the other is the diminishment of charging energy barrier as a result of increasing core size which facilitates interparticle charge transfer.

More recently, Murray *et al.*⁵² reported that temperature-induced core motion could also lead to drastic enhancement of the ensemble conductivity as a consequence of the thermal modulation of interparticle separations. Thus, it is very plausible that the transition observed in the present study (Fig. 5) can also be interpreted in a similar fashion by taking into account the contributing effects of thermally induced core motion as well as thermal activation of interparticle charge transfer. Both are clearly dependent upon the specific particle structures such as core size and protecting ligands (more discussion below).

Control experiments

We also measured the conductivity of the palladium nanoparticles passivated by alkanethiolates (Pd–SR) as a control experiment. The I – V curves are included in the ESI† (Fig. S2 and S3). Two aspects warrant special attention here. First, the conductivity of the Pd–SR nanoparticles is significantly smaller than that observed above with the Pd–C nanoparticles, despite comparable (or even shorter) chainlength of the organic capping

ligands and somewhat larger nanoparticle cores (Table 1). Second, the conductivity exhibits an exponential decay with ligand chainlength, signifying a hopping process in interparticle charge transfer, as observed previously (ESI† Fig. S3).^{44,48,53} In addition, the I - V characteristics were found to exhibit semiconductor behavior within the same temperature range where the conductivity increased with increasing temperature.

Note also that for arenethiolate-protected gold particles of similar sizes (protected by monolayers of benzylthiolate, phenylethylthiolate, phenylbutanethiolate, and cresolthiolate), the ensemble conductivities all exhibit semiconductor character within the temperature range of 223 K to 323 K, *i.e.*, the conductivity increases with increasing temperature, in sharp contrast to the Pd-C particles. Similar semiconductor behavior was also observed with *p*-toluenethiolate-protected Pd nanoparticles (ESI† Fig. S4).

Taken together, the above observations can be rationalized using Mott's model for metal-insulator transitions.⁵⁴ According to this model, a compressed lattice of hydrogen atoms is anticipated to exhibit metallic behavior when the interatomic distance approaches $\sim 4.5a_0$, where a_0 is the Bohr radius. By approximating nanoparticles as artificial atoms,

$$a_0 \sim \frac{\hbar}{\sqrt{2m^* \phi}}$$

where m^* is the effective mass of electrons, ϕ the barrier height, and \hbar Planck's constant. Thus, the transition of the conductance of a nanoparticle ensemble into the metallic domain only occurs when the interparticle charge transfer is sufficiently enhanced. This can be achieved by increasing particle core size (thus lowering the Coulombic barrier for interparticle charge transfer), decreasing particle-ligand contact resistance (hence enhancing electronic spilling beyond the metal cores), and/or raising ensemble temperature (by virtue of thermal activation and core thermal motions). Thus, whereas the aforementioned Pd-DP particles (Table 1) are substantially smaller than the Au-SR⁴⁷ and Ag-SR⁵⁰ particles that exhibit similar semiconductor-metal transitions with increasing temperature, the Pd-DP particles benefit from the strong Pd-C bonding and hence markedly reduced interfacial contact resistance that offset the core size effects.

Conclusions

Stable palladium nanoparticles have been prepared by passivation of the metal cores with Pd-C covalent linkages. Upon the addition of a strong reducing agent, the particles were produced by the reduction of palladium(II) precursors. Concurrently, the aliphatic radicals generated from the reduction of diazonium ligands formed the Pd-C linkages by taking advantage of the strong Pd-C bonding interactions. The nanoparticles were then characterized by TEM and various spectroscopic measurements. Interestingly, solid-state conductivity studies showed that the Pd-C particles exhibited drastically enhanced conductivity properties as compared to the alkanethiolate-protected counterparts. For instance, the Pd-BP particles exhibited metal-like temperature dependence of the conductivity, whereas the Pd-DP particle ensembles showed semiconductor-like character at temperatures lower than 180 K and metallic behavior at higher temperatures. In sharp contrast, only semiconductor characteristics were observed with the Pd-SR particles where the conductivity was

all found to increase with increasing temperature within the same temperature range. This study signifies the importance of metal-ligand linkages in the regulation of ensemble conductivity properties. Importantly, these unique characteristics can be rationalized using Mott's model for metal-insulator transitions.

Acknowledgements

This work was supported in part by the National Science Foundation (CHE-0456130 and CHE-0718170). TEM micrographs were acquired at the National Center for Electron Microscopy at the Lawrence Berkeley National Laboratory which is supported by the US Department of Energy.

References

- 1 A. C. Templeton, M. P. Wueling and R. W. Murray, *Acc. Chem. Res.*, 2000, **33**, 27.
- 2 R. L. Whetten, M. N. Shafiqullin, J. T. Houry, T. G. Schaaff, I. Vezmar, M. M. Alvarez and A. Wilkinson, *Acc. Chem. Res.*, 1999, **32**, 397.
- 3 A. C. Templeton, M. J. Hostetler, E. K. Warmoth, S. W. Chen, C. M. Hartshorn, V. M. Krishnamurthy, M. D. E. Forbes and R. W. Murray, *J. Am. Chem. Soc.*, 1998, **120**, 4845.
- 4 M. Brust, D. Bethell, C. J. Kiely and D. J. Schiffrin, *Langmuir*, 1998, **14**, 5425.
- 5 C. P. Collier, T. Vossmeier and J. R. Heath, *Annu. Rev. Phys. Chem.*, 1998, **49**, 371.
- 6 R. Shenhar and V. M. Rotello, *Acc. Chem. Res.*, 2003, **36**, 549.
- 7 S. W. Chen, A. C. Templeton and R. W. Murray, *Langmuir*, 2000, **16**, 3543.
- 8 M. Brust, M. Walker, D. Bethell, D. J. Schiffrin and R. Whyman, *J. Chem. Soc., Chem. Commun.*, 1994, 801.
- 9 S. W. Chen and R. W. Murray, *Langmuir*, 1999, **15**, 682.
- 10 M. S. Vickers, J. Cookson, P. D. Beer, P. T. Bishop and B. Thiebaut, *J. Mater. Chem.*, 2006, **16**, 209.
- 11 M. C. Tong, W. Chen, J. Sun, D. Ghosh and S. W. Chen, *J. Phys. Chem. B*, 2006, **110**, 19238.
- 12 W. Chen, J. Sun, D. Ghosh, M. C. Tong, F. Deng and S. W. Chen, *Electrochim. Acta*, 2007, **53**, 1150.
- 13 W. Chen, J. R. Davies, D. Ghosh, M. C. Tong, J. P. Konopelski and S. W. Chen, *Chem. Mater.*, 2006, **18**, 5253.
- 14 F. Mirkhalaf, J. Paprotny and D. J. Schiffrin, *J. Am. Chem. Soc.*, 2006, **128**, 7400.
- 15 R. W. Devenish, T. Goulding, B. T. Heaton and R. Whyman, *J. Chem. Soc., Dalton Trans.*, 1996, 673.
- 16 Y. Mizukoshi, K. Okitsu, Y. Maeda, T. A. Yamamoto, R. Oshima and Y. Nagata, *J. Phys. Chem. B*, 1997, **101**, 7033.
- 17 A. Nemamcha, J. L. Rehspringer and D. Khatmi, *J. Phys. Chem. B*, 2006, **110**, 383.
- 18 G. Cardenas, C. Munoz and V. Vera, *Bol. Soc. Chil. Quim.*, 1996, **41**, 235.
- 19 N. Nunomura, H. Hori, T. Teranishi, M. Miyake and S. Yamada, *Phys. Lett. A*, 1998, **249**, 524.
- 20 Y. J. Xiong, H. G. Cai, B. J. Wiley, J. G. Wang, M. J. Kim and Y. N. Xia, *J. Am. Chem. Soc.*, 2007, **129**, 3665.
- 21 A. B. R. Mayer and J. E. Mark, *Colloid Polym. Sci.*, 1997, **275**, 333.
- 22 O. Taratula, A. M. Chen, J. M. Zhang, J. Chaudry, L. Nagahara, I. Banerjee and H. X. He, *J. Phys. Chem. C*, 2007, **111**, 7666.
- 23 B. Chaudret, *C. R. Phys.*, 2005, **6**, 117.
- 24 S. W. Chen and K. Huang, *J. Cluster Sci.*, 2000, **11**, 405.
- 25 M. T. Reetz, M. Winter, R. Breinbauer, T. Thurn-Albrecht and W. Vogel, *Chem.-Eur. J.*, 2001, **7**, 1084.
- 26 F. L. Li, B. L. Zhang, S. J. Dong and E. K. Wang, *Electrochim. Acta*, 1997, **42**, 2563.
- 27 D. L. Lu and K. Tanaka, *J. Phys. Chem. B*, 1997, **101**, 4030.
- 28 S. W. Chen, K. Huang and J. A. Stearns, *Chem. Mater.*, 2000, **12**, 540.
- 29 F. P. Zamborini, S. M. Gross and R. W. Murray, *Langmuir*, 2001, **17**, 481.
- 30 L. S. Ott and R. G. Finke, *Coord. Chem. Rev.*, 2007, **251**, 1075.

-
- 31 D. Mann, A. Javey, J. Kong, Q. Wang and H. J. Dai, *Nano Lett.*, 2003, **3**, 1541.
- 32 P. Tarakeshwar and D. M. Kim, *J. Phys. Chem. B*, 2005, **109**, 7601.
- 33 Y. Woo, G. S. Duesberg and S. Roth, *Nanotechnology*, 2007, **18**, 095203.
- 34 D. R. Lide, *CRC handbook of chemistry and physics: a ready-reference book of chemical and physical data*, CRC Press, Boca Raton, FL, 2004.
- 35 H. H. Yang and R. L. McCreery, *Anal. Chem.*, 1999, **71**, 4081.
- 36 Z. L. Wang, *Adv. Mater.*, 2003, **15**, 1497.
- 37 Z. L. Wang, *J. Phys. Chem. B*, 2000, **104**, 1153.
- 38 J. A. Tossell, *Chem. Phys. Lett.*, 1998, **286**, 73.
- 39 M. J. Hostetler, J. E. Wingate, C. J. Zhong, J. E. Harris, R. W. Vachet, M. R. Clark, J. D. Londono, S. J. Green, J. J. Stokes, G. D. Wignall, G. L. Glish, M. D. Porter, N. D. Evans and R. W. Murray, *Langmuir*, 1998, **14**, 17.
- 40 J. A. Creighton and D. G. Eadon, *J. Chem. Soc., Faraday Trans.*, 1991, **87**, 3881.
- 41 R. M. Silverstein, G. C. Bassler and T. C. Morrill, *Spectrometric identification of organic compounds*, Wiley, Chichester, 1991.
- 42 Y. Song, A. S. Harper and R. W. Murray, *Langmuir*, 2005, **21**, 5492.
- 43 A. Badia, S. Singh, L. Demers, L. Cuccia, G. R. Brown and R. B. Lennox, *Chem.-Eur. J.*, 1996, **2**, 359.
- 44 W. P. Wuelfing and R. W. Murray, *J. Phys. Chem. B*, 2002, **106**, 3139.
- 45 L. Clarke, M. N. Wybourne, L. O. Brown, J. E. Hutchison, M. Yan, S. X. Cai and J. F. W. Keana, *Semicond. Sci. Technol.*, 1998, **13**, A111.
- 46 R. C. Doty, H. B. Yu, C. K. Shih and B. A. Korgel, *J. Phys. Chem. B*, 2001, **105**, 8291.
- 47 A. W. Snow and H. Wohltjen, *Chem. Mater.*, 1998, **10**, 947.
- 48 L. Y. Wang, X. J. Shi, N. N. Kariuki, M. Schadt, G. R. Wang, Q. Rendeng, J. Choi, J. Luo, S. Lu and C. J. Zhong, *J. Am. Chem. Soc.*, 2007, **129**, 2161.
- 49 S. Pradhan, D. Ghosh, L. P. Xu and S. W. Chen, *J. Am. Chem. Soc.*, 2007, **129**, 10622.
- 50 J. F. Sampaio, K. C. Beverly and J. R. Heath, *J. Phys. Chem. B*, 2001, **105**, 8797.
- 51 F. Remale and R. D. Levine, *Isr. J. Chem.*, 2002, **42**, 269.
- 52 J. P. Choi, M. M. Coble, M. R. Branham, J. M. DeSimone and R. W. Murray, *J. Phys. Chem. C*, 2007, **111**, 3778.
- 53 R. H. Terrill, T. A. Postlethwaite, C. H. Chen, C. D. Poon, A. Terzis, A. D. Chen, J. E. Hutchison, M. R. Clark, G. Wignall, J. D. Londono, R. Superfine, M. Falvo, C. S. Johnson, E. T. Samulski and R. W. Murray, *J. Am. Chem. Soc.*, 1995, **117**, 12537.
- 54 A. Zabet-Khosousi, P. E. Trudeau, Y. Suganuma, A. A. Dhirani and B. Statt, *Phys. Rev. Lett.*, 2006, **96**, 156403.